PROSIDING SNTTM XXII 2024
Volume 22, Tahun 2024, 02 Oktober 2024
e-ISSN 2623 0331
p-ISSN 3032 1972

Characterisation of Microfluidic Systems for Automated Extraction Device of DNA Sampling

Yudan Whulanza[a,b,1], Andriko Rasta Indriantomo[a], Cosmas Setto Nurdiyantoko[a], Ridho Irwansyah[a]

[a]Department of Mechanical Engineering, Faculty of Engineering, Universitas Indonesia, Depok, 16424
[b]Research Center for Biomedical Engineering, Faculty of Engineering, Universitas Indonesia, Depok, 16424

[1]yudan.whulanza@ui.ac.id

ABSTRACT

The development of microfluidic technology has a significant impact in a wide range of biomedical applications. Microfluidic devices allow sample processing in small quantities and reduce processing time. One important application is in molecular detection of DNA/RNA. Laboratory-on-Chip (LoC) for DNA detection technology has been developed to detect pathogens quickly and accurately in the field. This research aims to characterize microfluidic systems aided with piezoelectric micropump in various load scenarios. The scenarios were conducted in experimental and numerical simulation. Piezoelectric micropumps are chosen because they are small, lightweight, and can be controlled with high precision. The experiments were conducted using micropumps and various shapes and size of microfluidic chips with specific purposes such as mixing, reacting, and filtering. The results of the research showed that piezoelectric micropump has a linear relationship between flow rate and amplitude voltage. Here, the voltage applied is in the range of 20 V-100 V that corresponds with flow rate of 100-1600 µm/minute. In the case of scenario with mixing and reacting chambers has a margin of around 5% compared to the numerical simulations. Moreover, the filtration process provided a margin of around 25%. This study also demonstrated that the flow rate of 20-750 µL/minute resulted in a performance head of 0-6 mm. The performance of piezoelectric micropumps in a variety of loading conditions provided the basis for further development in further miniaturization system.

Keywords: microfluidic technology, moleculer detection, DNA/RNA, Labratory-on-Chip Device, piezoelectric microopump, miniaturization system.

Received 2 September 2024; Presented 2 Oktober 2024; Publication 20 Januari 2025
DOI: 10.71452/590886

INTRODUCTION

In recent decades, the advancement of microfluidic technology has become a focal point for various biomedical applications. Microfluidic devices require only a small amount of sample and can significantly reduce processing time [1]. Their applications range from cell engineering, drug screening, and in-situ diagnostic to creating relevant microenvironments. One of the critical applications of microfluidic technology is in the development of an early detection tool for specimen using a portable molecular technology device [2]. The target specimen can be a primary pathogen responsible for any disease, which can lead to significant health degeneration. Early detection of this pathogen is crucial for disease control and minimizing the associated health impact.

Molecular technology such as polymerase chain reaction (PCR) has been employed to detect the pathogen accurately. However, conventional PCR devices have several limitations, including pretreatment of the specimen namely the extraction of DNA which need specific laboratory apparatus and skilled personnel [2]. These challenges make field detection of DNA specimens difficult and impractical. To address these challenges, a portable DNA extraction tool based on lab-on-chip technology has been developed with accurate results [2].

This study integrates all steps in preparing DNA extraction in one platform that is easy to use and can be operated outside the laboratory. During the extraction phase, three different fluids-lysis-and-binding buffer, magnetic beads solution, and washing buffer are sequentially pumped into a chip. This necessitates a microfluidic system capable of delivering fluids with high precision and efficiently controllable in field settings. The selection of the type of micropump used in this system is therefore crucial. A piezoelectric micropump was selected for this study due to its several advantages that align with the needs of a portable DNA extraction device. Its small size and lightweight nature make it ideal for portable applications. Additionally, the piezoelectric micropump offers the ability to control its active and inactive pumping phases. The capability to simultaneously control four micropumps also facilitates the sequential flow of different fluid types into the microfluidic chip.

This study characterizes the piezoelectric micropump's performance in driving fluids through the

e-ISSN 2623 0331
p-ISSN 3032 1972

microfluidic system under various loading conditions using both direct experimentation and computational fluid dynamics (CFD) simulations. The results of this research are expected to provide a strong foundation for the further development of piezoelectric micropumps and portable DNA detection devices in various microfluidic systems and other biomedical applications.

METHODOLOGY

The configuration of three specimens required for insertion into the extraction chip is depicted in Figure 1. The extraction method comprises three stages: insertion of fluids for lysis, followed by washing and elution filtration. Fluid is introduced and removed in each process using a hand pipette. The present work investigates fluidic handling under various operating conditions.

Figure 1. Design of Extraction on Chip with three different liquid reagent

The microfluidic system experiment was conducted under five loading scenarios to evaluate the performance of the piezoelectric pump (MP6 series from Bartels Mikrotechnik GmbH) in controlling fluid flow within the microfluidic system. The five scenarios are as follows:

a) Microfluidic system without any load.
b) Microfluidic system with load using rhombic chamber chip.
c) Microfluidic system with load using reaction chamber chip.
d) Microfluidic system with load using open membrane chip.

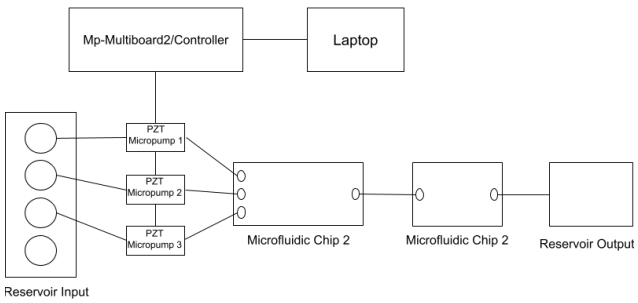

Figure 2. Schematic design of the proposed microfluidic transportation system

To establish the microfluidic transportation system, the following steps were undertaken. First, the microfluidic circuit was assembled to ensure all components were correctly positioned and connected. Subsequently, the interface software was downloaded and installed on the designated laptop. This software serves as the primary control platform for the system. Following the software installation, the controller-multiboard (MP-Highdriver4 pump driver from Bartel mikrotechnik) was connected to the laptop, enabling communication between the hardware components and the software interface (figure 2). Finally, all connections involving the micropump and sensors (SLF3x sensor) were verified within the interface software to ensure proper integration and functionality of the entire system.

EXPERIMENTAL SETUP

To conduct the microfluidic experiments, the following procedure was followed. First, the micropump was activated, and its frequency was set to 50 Hz with an initial voltage amplitude of 20 V using the control tab in the interface software. The waveform was then set to “Full-Sinusoidal” by selecting the leftmost option. “Next”, the “Timer” tab was used to program the micropump to operate for one minute. During this time, the flow rate data was recorded every second using the data logging tab. This data collection process was repeated for voltage variations from 20 V to 100 V, with adjustments made in increments of 10 V. After each load, the microfluidic system was thoroughly drained and cleaned to maintain a neutral condition for subsequent experiments. The data collection steps (1 through 4) were then repeated for each of the remaining loads.

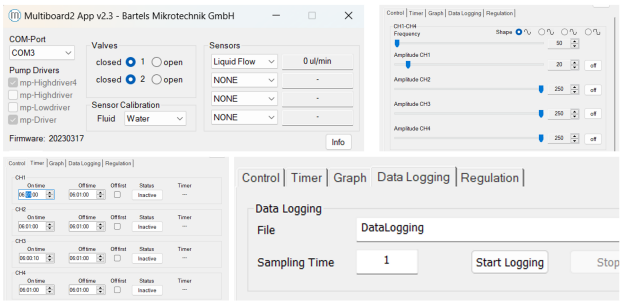

Figure 3. Arrangement of ports, driver, valve, and sensor in the micropump software

SIMULATION

In this simulation, a 2D model of the microfluidic system was developed for each loading scenario. The model was segmented into four distinct domains:

e-ISSN 2623 0331
p-ISSN 3032 1972

a. Inlet: The inlet domain represents the area where fluid initially enters the channel. In this model, the inlet is positioned on the left side of the channel.

b. Outlet: The outlet domain indicates the exit point where fluid leaves the system after traversing through it. In this model, the outlet is located on the right side of the channel.

c. Wall: The wall domain defines the boundaries of the simulation, constraining the movement of fluid within the system and ensuring that the flow remains within the designated area.

d. Porous Medium: The porous medium domain represents the area containing the porous material. This domain interacts directly with the fluid, influencing the flow behavior as the fluid passes through it.

CALCULATION

In the process of calculating the total head for a microfluidic system, several key components must be considered to ensure an accurate representation of the system's performance. These components include elevation head, pressure head, and other relevant factors. Below is a breakdown of how each component contributes to the total head calculation:

$$Pressure\ Head = \frac{P2-P1}{\rho g} \quad (1)$$

where:
$P1$ = Initial Fluid Pressure (Pa)
$P2$ = Final Fluid Pressure (Pa)
ρ = Fluid Density (kg/m³)
g = Gravitational Acceleration (m²/s)

The velocity profile data above can then be used to calculate the flow rate at the outlet using the following equation:

$$Q = v.A \quad (2)$$

where:
Q = Flow Rate of the fluid (m³/s)
v = Fluid Velocity (m/s)
A = Cross-sectional Area of the Pipe (m²)

$$Velocity\ Head = \frac{v^2}{2g} \quad (3)$$

where:
v = Fluid Velocity (m/s)
g = Gravitational Acceleration (m²/s)

$$Head\ Loss, H_{Loss} = f.\frac{L}{D}.\frac{v^2}{2g} \quad (4)$$

where:
f = Darcy Friction Factor
L = Length of the Pipe (m)
D = Diameter of the Pipe (m)
v = Fluid Velocity (m/s)
g = Gravitational Acceleration (m²/s)

Mathematically, the total head can be expressed as the sum of all these individual components using the following formula:

$$H_{total} = H_{elevation} + H_{Pressure} + H_{Velocity} + H_{loss} \quad (5)$$

The microfluidic system parameters for each example are as defined below:

Table 1. Numerical simulation parameter

Parameter	Symbol	Value
Elevation	z_2-z_1	0
Viscosity (water)	η	0.890 mPa·s
Density (water)	ρ	997 kg/m³
Length distance no load Length distance load 1 Length distance load 2 Length distance load 3 Length distance load 4	L	0.0013 m
Diameter of hose	D	

RESULTS AND DISCUSSION

Micropump Characterization

Figure 4 illustrates several electronic components discussed in this work, including reservoir, extraction, reaction chamber, and open membrane chips. This arrangement of chips was contained within a self-designed and constructed frame, allowing us to integrate all the chips into a single platform together with the micropump, sensor, and controller-board. The controller board must be linked to software as the primary interface of a laptop or personal computer. The specimen and all three reagents were inserted into a reservoir that was mechanically linked to the open chamber chip. The chamber chip was connected to the micropump to direct the flow to either the extraction chip, reaction chamber chip, or a series arrangement comprising both chips. The efficiency of the micropump was evaluated by means of the flow sensor.

e-ISSN 2623 0331
p-ISSN 3032 1972

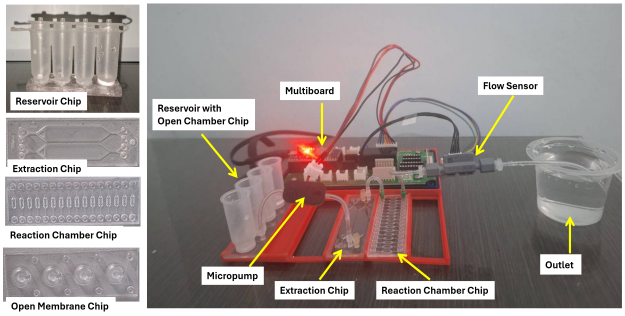

Figure 4. Arrangement of different microchips as load in the experimental configuration

Before conducting the flow rate measurement experiment, sensor calibration is first performed to ensure that the captured data is precise and accurate. Calibration is done by comparing the flow rate data from the microfluidic system experiment without load, as read by the sensor, with the flow rate data obtained by dividing the volume of fluid exiting the system by the duration of the experiment (figure 5a). The volume of fluid exiting is measured using a measuring cylinder, and the experiment duration is measured using the timer setting on the micropump software interface (Bartel MP-6).

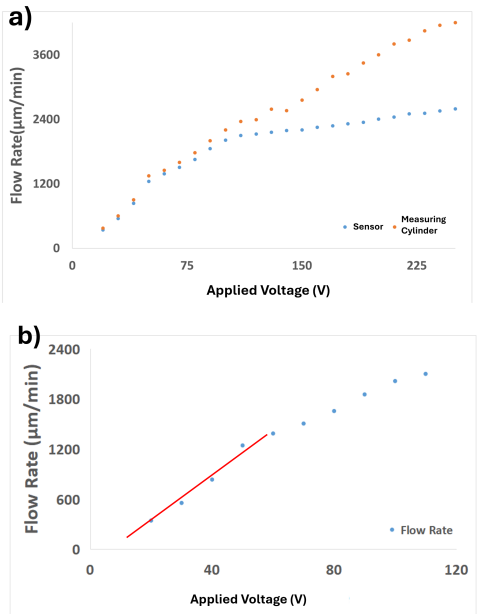

Figure 5. The flow rate calibration was obtained by micropumping, utilizing a sensor and measuring cylinder. The result was obtained within the selected range of applied voltage in this empirical study.

Figure 5 shows the pump characterisation curve derived from the flow rate produced with the applying voltage. A positive correlation between flow rate and amplitude voltage is observed from the curve illustrated. Consequently, the flow rate exhibits a positive correlation with the amplitude of the voltage. The observed rise in magnitude indicates a strong linear relationship between the applied voltage and the consequent flow rate, therefore suggesting that the piezoelectric pump system functions with a high level of efficiency within the specified voltage range.

Figure 5a also demonstrates that in the case of an amplitude of 110 V, there exists a somewhat significant disparity about 10%. Thus, the amplitude values employed for this microfluidic system experiment followed a range of 20 V to 120 V. This characterization suggests that the flow sensor being utilized achieves optimal accuracy when the flow rate is at its maximum value of 1,200 mm/min. This was shown as a linear trend until that flowrate, afterwards transitioning to a curvilinear trend (figure 5b).

Comparative Result of Experimental and Numerical Simulation for All Scenarios

The entrance flow rate parameter in the numerical simulation using COMSOL software was modified to align with the flow meter readings acquired from the experiment investigating the unloaded microfluidic system. In order to represent the velocity profile for each loading scenario, the simulation utilized a laminar flow interface. The velocity profiles obtained from the computational fluid dynamics (CFD) simulation are as depicted in figure 6.

e-ISSN 2623 0331
p-ISSN 3032 1972

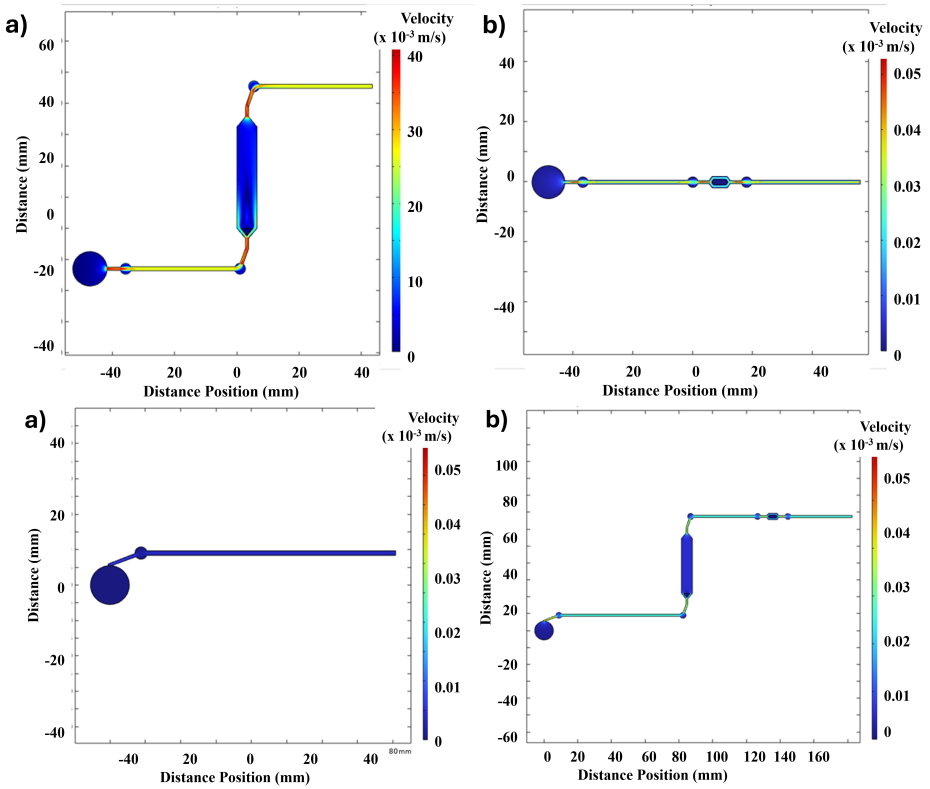

Figure 6. Numerical simulation results under different experimental loads

Following that, the flow rate values of the input were altered in accordance with the flow rate data obtained from the experiment involving the unloaded system. The microfluidic system experiment was conducted under four distinct loading settings. In addition, the voltage data obtained from the experiment in which the system was not loaded was utilized to modify the micro-pump. This was done to guarantee that the input flow rate stayed constant across all loading scenarios. The figure 7 depicts a comparison between the findings of the experiment and the simulation that was performed using numerical simulation software.

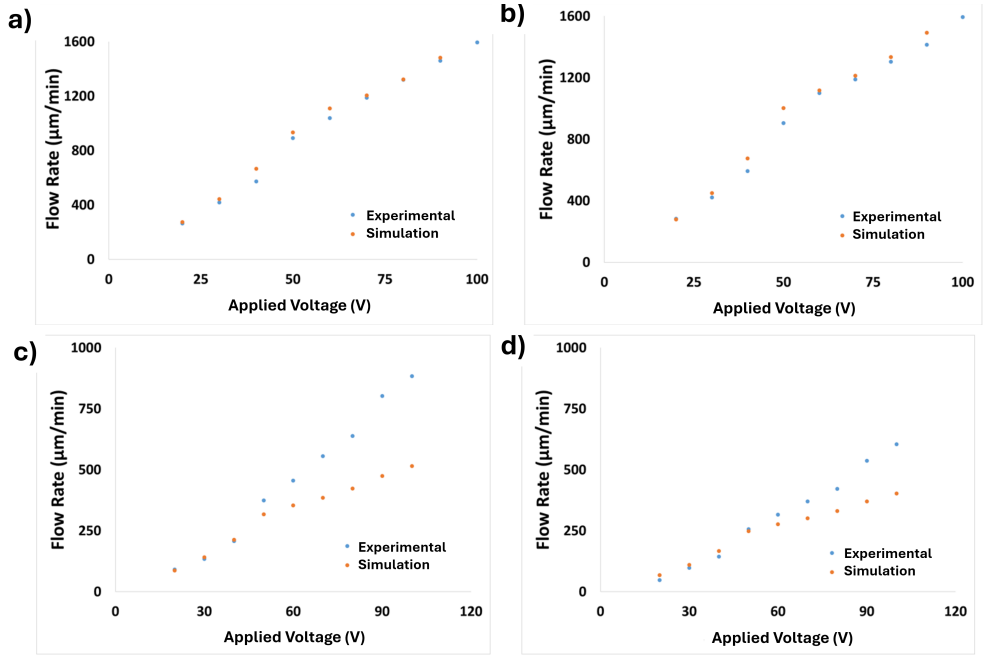

Figure 7. Comparative flow rate is obtained for different loads in both experimental and simulated settings.

e-ISSN 2623 0331
p-ISSN 3032 1972

Figure 8 illustrates that all four loading situations display a positive trend between flow rate and amplitude voltage. This tendency is comparable to the findings that were obtained from the experiment that was conducted without any loading. In the first scenario, the microfluidic system with the rhombic chamber load exhibits a difference of 8.25%; in the second scenario, the system with the reaction chamber load exhibits a difference of 9.71%; in the third scenario, the system with the open membrane chip load exhibits a difference of 59.71%; and in the fourth scenario, the system with three loads simultaneously exhibits a difference of 54.17%.

System Characterization

To fully evaluate the effectiveness of a microfluidic system, it is essential to determine the system head, which is the net pressure difference that the pump needs to overcome to maintain fluid flow inside the network. The determination of the system head (H) considers several factors, including the resistance shown by the micro-channels, the viscosity of the fluid, and any additional external sources such as gravity or pressure gradients. The total head (H) is evaluated by comparing it to the flow rate (Q), which measures the volume of fluid flowing through the system during a specific time period as in table 2.
The relationship between the system head and the flow rate normally exhibits non-linearity, as the required head significantly rises with increasing flow rate due to the increasing resistance encountered by the fluid in the microchannels. By graphing a pump characteristic curve, engineers can assess the operational efficiency of a microfluidic pump by observing the relationship between the total head (H) and the flow rate (Q). By ensuring that the pump provides sufficient pressure to meet the system's requirements without exceeding energy consumption or risking damage caused by excessive pressure buildup, this study enables the optimization of system design.

Table 2. Result of pressure head calculation according to equation 1

Amplitude Voltage	Pressure Head (m)				
	no load	Rhombic Chamber	Reaction Chamber	Open Membrane	3 Load
20	1.30E-04	1.00E-04	1.07E-04	3.45E-05	1.82E-05
30	2.10E-04	1.58E-04	1.60E-04	5.11E-05	3.69E-05
40	3.16E-04	2.17E-04	2.24E-04	7.88E-05	5.47E-05
50	4.71E-04	3.38E-04	3.43E-04	1.42E-04	9.70E-05
60	5.25E-04	3.93E-04	4.17E-04	1.73E-04	1.20E-04
70	5.70E-04	4.50E-04	4.51E-04	2.11E-04	1.40E-04
80	6.27E-04	5.00E-04	4.94E-04	2.42E-04	1.60E-04
90	7.02E-04	5.53E-04	5.36E-04	3.04E-04	2.04E-04
100	7.63E-04	6.04E-04	6.04E-04	3.35E-04	2.29E-04

In order to calculate the total head of a fluid system, one must aggregate all the pertinent components that contribute to the energy needed for fluid movement within the system. These components, namely elevation head, pressure head, and velocity head, each correspond to distinct types of energy that impact the movement of fluid. In aggregate, they offer a comprehensive representation of the overall energy per unit mass of the fluid required to surmount the resistance of the system and attain the intended flow rate.
After the determination of these total head values, the results are graphically represented with total head (H) on the vertical axis and flow rate (Q) on the horizontal axis. The figure 8 shows a crucial instrument for illustrating the correlation between the desired total head of the system and the fluid's flow rate. In general, the figure illustrates a non-linear correlation, where higher flow rates require a larger total head because of the expanded resistance within the microchannels. The obtained curve offers a straightforward depiction of the system's performance when subjected to different operational constraints.

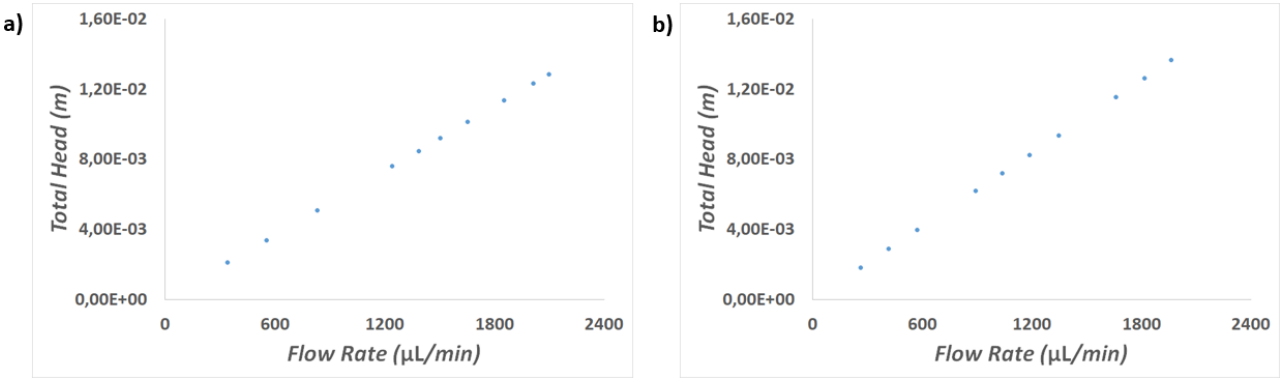

e-ISSN 2623 0331
p-ISSN 3032 1972

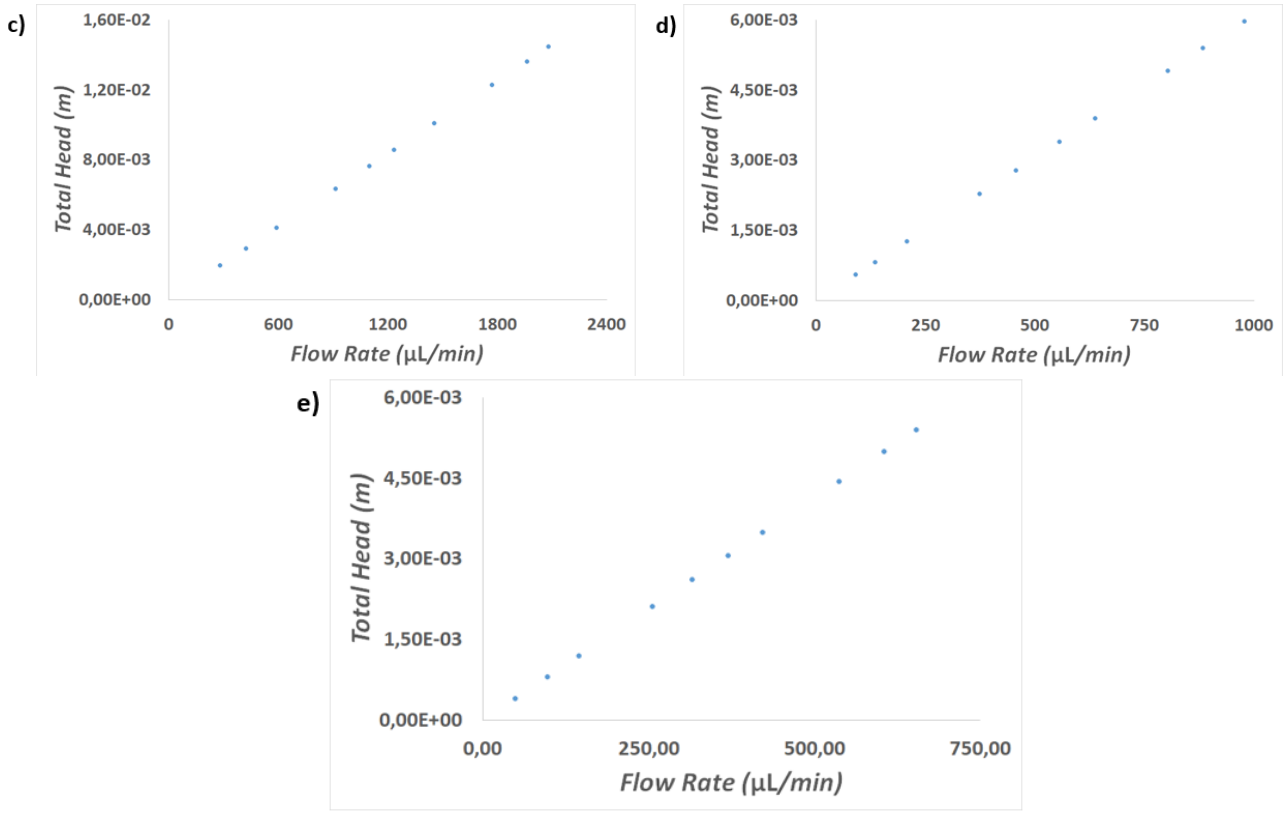

Figure 8. The experimental results determine the overall head of the different loads

The graph of total head (H) versus flow rate (Q) provides us with the system head curve, a critical tool in understanding the performance requirements of the microfluidic system. figure 8 illustrates the relationship between the flow rate that the system needs to achieve and the total head the micropump must overcome to maintain that flow. The system head curve effectively serves as a performance benchmark, showing how much energy the pump must supply in terms of pressure and resistance to move fluid through the microchannels.

Upon examining the graph across the five loading cases, a clear positive trend emerges: as the flow rate increases, so does the total head that the micropump must overcome. This trend is expected because higher flow rates inherently lead to greater frictional resistance within the microfluidic channels, as well as potentially higher-pressure differences that the pump needs to counterbalance. The system requires more energy input to push the fluid through the microchannels at higher velocities, especially in systems with narrow or complex geometries.

Each case on the graph reflects a different set of conditions, such as variations in fluid properties, microchannel dimensions, or external influences. Despite these differences, the general trend remains consistent: the greater the demand for flow, the higher the total head required. This pattern underscores the importance of selecting an appropriately sized and powered micropump to meet the system's flow rate requirements without causing inefficiencies or overburdening the pump.

This positive correlation between flow rate and total head is a fundamental characteristic of microfluidic systems. It provides engineers with crucial insights for optimizing system design, ensuring that the pump can meet the varying demands of the system under different operating conditions. By studying the system head curve, one can evaluate whether the micropump can handle peak flow rates, manage energy consumption, and avoid potential system failures due to insufficient pressure generation.

CONCLUSION

1. In each loading case, the MP-6 piezoelectric micropump demonstrated a linear relationship between flow rate and amplitude. The experiments were conducted by varying the voltage applied to the micropump. The voltage range used was between 20 V and 100 V, which was determined based on the effectiveness of the flow rate sensor in capturing the data received. A significant

e-ISSN 2623 0331
p-ISSN 3032 1972

increase in flow rate was observed with the increase in applied voltage, indicating that the microfluidic system using the piezoelectric micropump operates with high efficiency within the given voltage range.

2. The experimental results showed lower flow rates compared to the numerical simulation results in the loading cases using the rhombic chamber and reaction chamber. However, the experimental flow rate was observed to be higher in the loading case using the open membrane chip, with a significant difference. Specifically, in the loading case using the rhombic chamber, a difference of 4.29% was observed, in the loading case using the reaction chamber, the difference was 4.62%, in the loading case using the open membrane chip, the difference was 32.59%, and in the loading case using all three loads simultaneously, the difference was 24.15%. These differences may be attributed to the neglect of hydrostatic pressure in the CFD simulations and potential errors in membrane parameter modeling. Nevertheless, a positive trend between flow rate and voltage was observed in both methods, indicating consistent micropump performance.

3. The graph of total head (H) vs flow rate (Q) exhibited a linear relationship, indicating that the total head the micropump must overcome increases with the flow rate. This trend was observed in all the loading cases conducted.

REFERENCE

[1] Daghighi, Yasaman. “Microfluidic Technology And Its Biomedical Applications.” Journal of Thermal Engineering, vol. 1, no. 07, 2015, pp. 621-626. 1.

[2] Josephin, A., Whulanza, Y., Rahman, S.F., Lischer, K., Surya, M.I., Martiansyah, I., Rahman, W. and Hashim, U., 2024. Easy extraction of Ganoderma boninense liquid sample using portable on-chip device. Indonesian Journal of Biotechnology, 29(1), pp.33-39.

[3] Zhao, Yimeng, et al. “Microfluidic Actuated and Controlled Systems and Application for Lab-on-Chip in Space Life Science.” 2023, vol. 3, no. 08, https://doi.org/10.34133/.

[4] Lake, John R., et al. “Low-cost feedback-controlled syringe pressure pumps for microfluidics applications.” PLoS ONE 12 (4): e0175089., 2017, https://doi.org/10.1371/journal.Pone.0175089.

[5] Cheng Huo et al. “Micropumps for Microfluidic Devices and BioMEMS.” 2020 J. Phys.: Conf. Ser. 1626 012040

[6] Castillo-León, Jaime, and Winnie E. Svendsen, editors. Lab-on-a-Chip Devices and Micro-Total Analysis Systems: A Practical Guide. Springer International Publishing, 2014, https://www.researchgate.net/publication/281080765Lab-on-a-ChipDevicesandMicro-TotalAnalysisSystemsAPracticalGuide.

[7] Bao, Qibo et al. “A Novel PZT Pump with Built-in Compliant Structures.” MPDI, 2019.

[8] Ali, Faisal et al. “Performance Analysis of MP6 micro pumps (Piezoelectric Diaphragm) for Remote Automated Water Quality Monitoring.” i-coste.org.

[9] Kang Ma, Hsiao et al. “Development of a piezoelectric micropump with novel separable design for medical applications.” Sensors and Actuators A: Physical, 2015, https://www.sciencedirect.com/journal/sensors-and-actuators-a-physical.

[10] Whulanza, Y., Irwansyah, R., & Warjito (2023). Produk mikro dan teknologi lab-on-chip. UI Publishing.

[11] White, F. M. (2016). Fluid Mechanics (8th ed.). McGraw-Hill Education.

[12] Fox, R. W., McDonald, A. T., & Pritchard, P. J. (2015). Introduction to Fluid Mechanics (8th ed.). John Wiley & Sons.